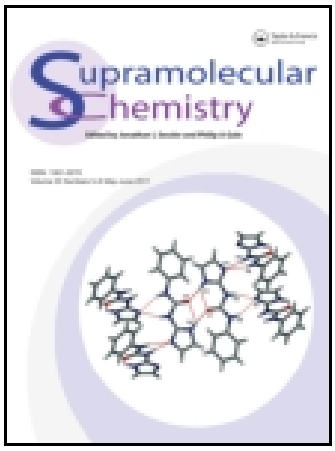

Supramolecular Chemistry
Publication details, including instructions for authors and subscription information:
http://www.tandfonline.com/loi/gsch20

Novel supramolecular columnar liquid crystals based on thiosemicarbazides

E. Y. Elgueta [a], M. L. Parra [a], J. Barberá [b], J. M. Vergara [a] & J. A. Ulloa [a]

[a] Departamento de Química Orgánica, Facultad de Ciencias Químicas, Universidad de Concepción, Casilla 160-C, Concepción, Chile

[b] Departamento de Química Orgánica, Facultad de Ciencias-Instituto de Ciencia de Materiales de Aragón, Universidad de Zaragoza-C.S.I.C., 50009, Zaragoza, Spain

Published online: 03 Nov 2011.

To cite this article: E. Y. Elgueta, M. L. Parra, J. Barberá, J. M. Vergara & J. A. Ulloa (2011) Novel supramolecular columnar liquid crystals based on thiosemicarbazides, Supramolecular Chemistry, 23:11, 721-730, DOI: 10.1080/10610278.2011.622390

To link to this article: http://dx.doi.org/10.1080/10610278.2011.622390

Supramolecular Chemistry
Vol. 23, No. 11, November 2011, 721–730

Novel supramolecular columnar liquid crystals based on thiosemicarbazides

E.Y. Elgueta[a], M.L. Parra[a]*, J. Barberá[b], J.M. Vergara[a] and J.A. Ulloa[a]

[a]*Departamento de Química Orgánica, Facultad de Ciencias Químicas, Universidad de Concepción, Casilla 160-C, Concepción, Chile;* [b]*Departamento de Química Orgánica, Facultad de Ciencias-Instituto de Ciencia de Materiales de Aragón, Universidad de Zaragoza-C.S.I.C., 50009 Zaragoza, Spain*

(*Received 4 July 2011; final version received 7 September 2011*)

Novel liquid crystal materials based on 3,4-di-*n*-alkoxybenzoylthiosemicarbazides (**3a**–**h**, $n = 5–10$, 12, 14) were synthesised. The mesomorphic properties of these compounds were characterised and studied by differential scanning calorimetry, polarising optical microscopy and X-ray diffraction. Compound **3a** did not show mesomorphic properties; **3b** shows a monotropic hexagonal columnar (Col_h) phase. Compounds **3c**–**h** display an enantiotropic Col_h phase. The mesomorphic properties were found to be dependent on the length of alkoxy side chains. In *N*,*N*-dimethylformamide solution, all the compounds displayed a room temperature emission with λ_{max} at 361–332 nm. A thermogravimetric analysis also was performed.

Keywords: thiosemicarbazides; columnar liquid crystals; mesomorphism

1. Introduction

Supramolecular chemistry is the chemistry of the non-covalent intermolecular interaction, covering the structures and the functions of the entities formed by the association of two or more chemical species (*1*). Non-covalent interactions include hydrogen bonding, electrostatic (ion–ion, ion–dipole and dipole–dipole) interactions, π–π stacking interactions, the Van der Waals interactions and hydrophobic–hydrophilic effects along with others (*2*). These interactions are essential to organise highly ordered superstructures. In liquid crystals, these interactions contribute to create rigid cores in both calamitic and disk-like molecules (*3–10*). Among the non-covalent interactions described above, hydrogen bond is the most important non-covalent interaction to design supramolecular architectures (*11*) due to its directionality, stability, selectivity and reversibility (*12*). Special attention has been given to intermolecular hydrogen bonding, which has been shown to efficiently promote molecular ordering and stability in a liquid crystalline phase by allowing it to assume the shape of a large disk in discotic liquid crystals (*13*).

Intermolecular hydrogen bonding plays an important role in mesophase formation in the hydrazide derivatives (*14–19*), which are the most common precursors in the synthesis of 1,3,4-oxadiazole- and 1,3,4-thiadiazole-based liquid crystalline derivatives. Thiosemicabazides and their related heterocyclic compounds have been found to possess many important biological activities. Some of them have been found to be useful as herbicides, insecticides and plant growth regulators (*20–23*). However, there are no reports on thiosemicabazide derivatives showing liquid crystalline properties.

In this work, we report the synthesis, characterisation and mesomorphic properties of novel liquid crystals based on thiosemicarbazides, specifically the 3,4-*n*-dialkoxybenzoylthiosemicarbazides (series **3a**–**h**). Previously, we have reported non-mesomorphic 4-*n*-alkoxybenzoylthiosemicarbazides (*24*, *25*) (see Figure 2). In contrast to those compounds, the thiosemicarbazides reported here display columnar liquid crystal behaviour, which can be attributed both to the presence of two lateral alkoxy chains and the intermolecular hydrogen bonding which in turn stabilise supramolecular structures in a columnar order. It has been suggested that the formation of hydrogen bonds promote molecular ordering and stability in a liquid crystalline phase, thus explaining the appearance of columnar mesophases (*13*). In the present hydrogen-bonded systems, self-assembled columnar liquid crystalline phases are not formed *via* discotic molecules, but rather by supramolecular 'discs' as building blocks generated through intermolecular hydrogen bonding (*26*, *27*). To our knowledge, the prepared compounds are the first thiosemicarbazide derivatives exhibiting liquid crystalline behaviour in particular Col_h phase. Special attention was paid to the columnar phase behaviour, the effect of the length of the terminal alkoxy chains on the phase behaviour, the mesophase structure and the fluorescence

*Corresponding author. Email: mparra@udec.cl

ISSN 1061-0278 print/ISSN 1029-0478 online

http://dx.doi.org/10.1080/10610278.2011.622390
http://www.tandfonline.com

of new compounds. Liquid crystals displaying columnar mesophases are very important due to their great potential application in semiconducting and photoconducting devices, light-emitting diodes and sensors based on their two essential virtues: their anisotropic charge carrier transport capability and the 'large area uniformity' (*28*).

Two points must be noted. First, series **3a**–**h** compounds open an interesting possibility for the design of 2-amino-1,3,4-thiadiazole and/or 2-amino-1,3,4-oxadiazole derivatives, because the thiosemicarbazide derivatives are the precursors in the synthesis of these heterocycles, which might exhibit interesting mesomorphic and luminescence behaviour. Second, the 2-amino-1,3,4-thiadiazole and/or 2-amino-1,3,4-oxadiazole derivatives can be used as precursors in the preparation of amides and/or Schiff's bases leading to polycatenar liquid crystals (*24*, *25*).

2. Results and discussion

2.1 Synthesis

The synthesis of the series **3a**–**h** compounds is outlined in Scheme 1. The thiosemicarbazide derivatives of **3a**–**h** were synthesised starting with the alkylation of methyl 3,4-dihydroxybenzoate with 1-bromoalkane ($n = 5–10$, 12, 14) under basic conditions yielding the corresponding methyl 3,4-*n*-dialkoxybenzoate **1a**–**h** and proceeding with condensation with hydrazine hydrate, yielding 3,4-*n*-dialkoxyphenylhydrazides **2a**–**h**; these were reacted with ammonium thiocyanate in concentrated HCl, leading to the formation of the 3,4-*n*-dialkoxybenzoylthiosemicarbazides **3a**–**h** (*24*, *25*, *30*).

2.2 Mesomorphic properties

The phase transition temperatures and enthalpies of the thiosemicarbazides **3a**–**h**, differing only in the number of the carbon atoms in the side chains, are listed in Table 1.

As can be seen from Table 1, except for the case of **3a**, which is non-mesomorphic, all the compounds of series **3** exhibit mesomorphic properties. The homologue **3b** displays a monotropic columnar hexagonal mesophase (Col_h), whereas the other homologues ($n = 7–10$, 12, 14) show an enantiotropic columnar hexagonal mesophase (Col_h). The textures observed by polarising optical microscopy (POM), on cooling from the isotropic liquid, are consistent with the presence of columnar mesomorphism. Microphotographs of the texture observed for the compounds **3b**–**h** are shown in Figure 1.

The data collected in Table 1 show the effect of increasing the length of the side chains. The fact that a columnar phase is observed for compounds **3b** (monotropic) and **3c**–**h** (enantiotropic) is evidence of the direct dependence of the mesomorphism of thiosemicarbazides on the length of the alkoxy chains.

The melting temperatures of compounds in series **3a**–**h** are in the range 129–174°C. No liquid crystalline phase was observed for compound **3a**, which has the higher melting point (174°C). Increasing the chain length results in a lowering of the melting point and in a favouring of the mesomorphic properties (monotropic for compound **3b** and enantiotropic for compounds **3c**–**h**).

With respect to the clearing temperatures and mesophase ranges, all of these compounds display moderate clearing temperatures and it is important to note their broad mesophase ranges. The clearing temperatures increase with the length of the alkoxy chains from 173°C for **3c** to 182°C for **3f** (*n*-pentyloxy to *n*-decyloxy chain); however, when the alkoxy chains increase by two carbon atoms in **3g** (*n*-dodecyloxy) and four carbon atoms in **3h** (*n*-tetradecyloxy), this results in a lowering of the clearing temperature compared with compound **3f**, being the lowest for compound **3h**. The homologue **3f**, containing *n*-decyloxy chains, has a broader mesomorphic range (38°C) than the homologues **3c** (20°C), **3d** (26°C), **3e** (31°C), **3g** (19°C) and **3h** (17°C). The same tendency as for the clearing temperatures is

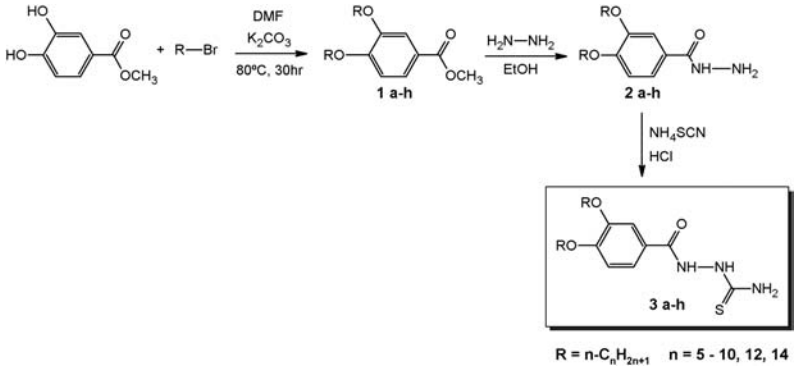

Scheme 1. Synthetic route for thiosemicarbazides of series **3a**–**h**.

Table 1. Phase transition temperatures (°C), enthalpies (J g^{-1}, in parentheses) as determined by DSC, scanning rate 10°C min^{-1}, ΔT (°C, mesomorphic range), T_{id} (°C, first step of decomposition), T_{sd} (°C, second process of decomposition) and T_{wd} (°C, whole decomposition process) for compounds of series **3a**–**h**.

Compound	Phase transitions	ΔT	T_{id}	T_{sd}	T_{wd}
3a ($n = 5$)	Cr 174 (88.9) I	–	191	242	603
3b ($n = 6$)	Cr 162 (80.7) I I 151 (3.0) Col_h –	–	194	247	604
3c ($n = 7$)	Cr 153 (79.3) Col_h 173 (2.3) I I 165 (2.5) Col_h –	20	187	239	604
3d ($n = 8$)	Cr 152 (75.0) Col_h 174.7 (2.4) I I 168 (–) Col_h –	26	189	239	589
3e ($n = 9$)	Cr 149 (74.8) Col_h 180 (2.8) I I 172 (–) Col_h –	31	185	233	603
3f ($n = 10$)	Cr 144 (60.9) Col_h 182 (2.2) I I 175 (–) Col_h –	38	190	240	594
3g ($n = 12$)	Cr 133 (58.3) Col_h 152 (–) I I 150 (–) Col_h –	19	193	268	589
3h ($n = 14$)	Cr 129 (50.4) Col_h 146 (2.2) I I 148 (3.0) Col_h –	17	195	265	605

Note: Cr, crystal phase; Col_h, hexagonal columnar phase; I, isotropic phase; –, enthalpy transition not observed.

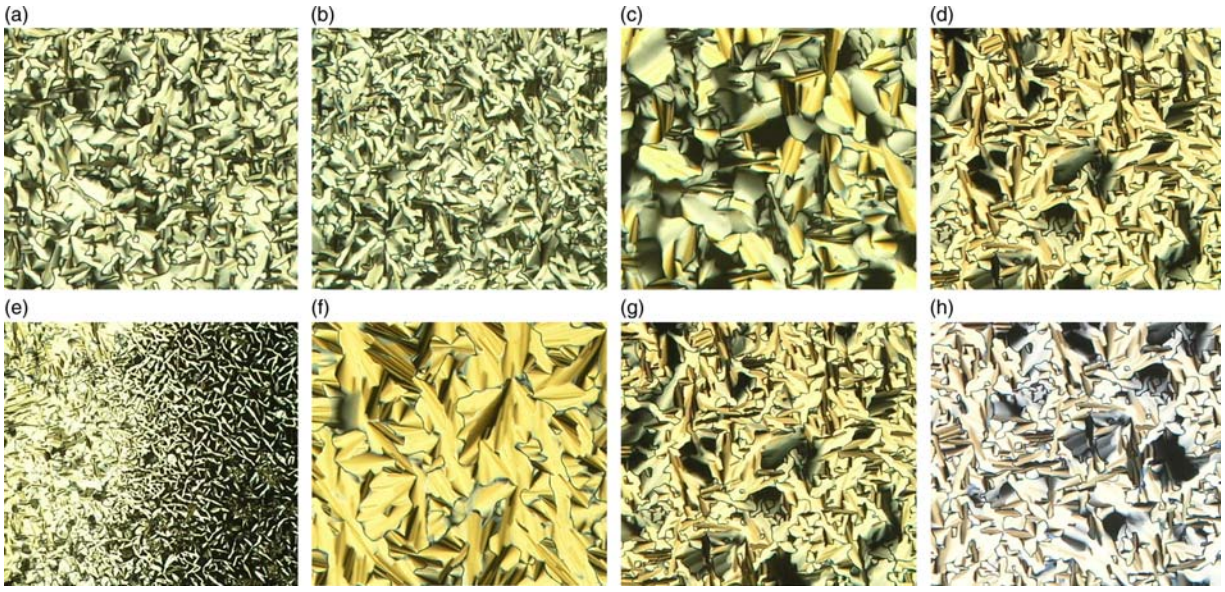

Figure 1. Optical textures of the columnar hexagonal mesophase obtained on cooling for compounds **3b** at 129°C (a), **3c** at 154°C (b), **3d** at 143°C (c), **3e** at 156°C (d), **3f** at 145°C (e) and 121°C (f), **3g** at 102°C (g) and compound **3h** at 113°C (h).

observed for the mesomorphic temperature ranges. Thus the mesomorphic range increases with the length of the alkoxy chains from **3c** to **3f** and decreases for compounds **3g** and **3h**, the homologue **3h**, with two *n*-tetradecyloxy chains, having the lowest mesomorphic range. All of these observations may well be indicative of the higher degree of disorder attributable to the longer flexible alkoxy chains in homologues **3g** and **3h**.

Upon cooling to room temperature (RT) no crystallisation occurred for compounds **3b**–**h**; only the isotropic-to-mesophase transition was observed and the columnar order was kept at RT, which is also indicative of a high degree of disorder due to the flexible alkoxy chains, which hinders crystallisation.

As mentioned above, we have previously reported the synthesis of non-mesomorphic 4-*n*-alkoxybenzoylthiosemicarbazides (**Ia**–**f**, see Figure 2) (*24*, *25*). The only difference between the thiosemicarbazides **3a**–**h** described here and the thiosemicarbazides **Ia**–**f** is the number of alkoxy chains attached to the benzene ring. The thiosemicarbazides **3a**–**h** have two *n*-alkoxy chains, whereas the thiosemicarbazides (**Ia**–**f**) have only one

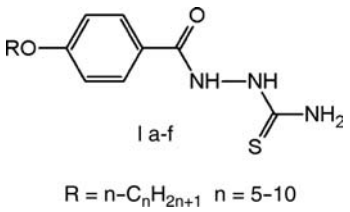

Figure 2. Structure of reported 4-*n*-alkoxybenzoylthiosemicarbazides (**Ia**–**f**).

n-alkoxy chains. The latter are non-mesomorphic and only a crystal–isotropic transition was observed at ~200°C. On the other hand, the thiosemicarbazides of series **3a**–**h** have lower melting points than thiosemicarbazides **Ia**–**f** and, with the exception of homologue **3a**, they are mesomorphic displaying both monotropic (**3b**) and enantiotropic (**3c**–**h**) mesomorphism. These results illustrate the importance of the influence of the number of the side chains in the occurrence of columnar hexagonal order. Probably, the mesomorphic properties of benzoylthiosemicarbazides described here are the result of the hydrogen bond interactions of the thiosemicarbazide group, which in turn reinforce the columnar organisation (*30*).

2.3 Thermogravimetric analysis

The thermogravimetric analysis (TGA) curves of solid samples of **3a**–**h** are given in Figure S1 (Supporting Information, available online). All solid samples showed no apparent weight loss between 20 and ~190°C, indicative of the absence of occluded solvent of crystallisation. All of them started to lose weight at around 190°C (~1% of weight loss) to 250°C (~10% of weight loss) in a two-step process and the whole decomposition process completed near 600°C. As can be seen in Table 1, the decomposition of the thiosemicarbazides **3a**–**h** starts at a temperature a few degrees above the isotropic transition: about 17°C for **3a**, 32°C for **3b**, 14°C for **3c**, 14°C for **3d**, 5°C for **3e**, 8°C for **3f**, 41°C for **3g** and 49°C for **3h**. These differences reflect the evolution of the isotropic transition temperatures. For example, compounds **3e** and **3f** have the highest clearing temperatures whereas compounds **3g** and **3h** have the lowest clearing temperatures. Therefore, decomposition starts closer to the isotropic transition for the former. This analysis is valid for all homologues in series **3a**–**h**.

2.4 X-ray diffraction studies

The mesophases of compounds **3b**–**h** were studied by X-ray diffraction (XRD) at RT and at high temperature. In view of the thermal behaviour of the compounds and, in particular, the absence of crystallisation on cooling from the isotropic liquid or from the mesophase, the first set of X-ray experiments were performed at RT on thermally treated samples of the seven compounds. The thermal treatment consisted of heating the pristine crystalline samples to the isotropic liquid or to the mesophase at a temperature slightly lower than the clearing point. Under these conditions all the compounds developed their liquid crystal phase, including **3b**, the mesophase of which is monotropic and could only be obtained upon cooling from the isotropic liquid. In spite of the metastable character of the mesophases at RT, all of them remained during the time of the X-ray experiments.

After the study at RT, the mesophases were studied at a temperature comprised between the melting and the clearing point, except for **3b**, the mesophase of which could not be studied at high temperatures because of its tendency to crystallise. It was observed that this tendency is more marked at high temperatures than at RT.

Table 2 gathers the structural parameters deduced from the X-ray measurements. The measured spacing and the corresponding indexation are collected in Table S1 (Supporting Information, available online). All the diffractograms are consistent with a hexagonal columnar mesophase. At RT this is unambiguously revealed by the presence in the small-angle region of most patterns of a set of sharp maxima with reciprocal spacing in the ratio $1:3^{1/2}:2$. These peaks correspond, respectively, to (1 0), (1 1) and (2 0) reflections from a 2D hexagonal lattice. The hexagonal lattice constant a is deduced from these reflections and its value for each compound is shown in Table 2, as well as the cross-section area of the hexagonal unit cell S calculated from a. It can be observed that these parameters evolve in a logical fashion and increases steadily upon growing the length of the hydrocarbon chains.

Table 2. Structural parameters of the mesophases of compounds **3b**–**h** determined by XRD; a is the lattice constant of the Col_h phase; S is the cross-section area of the hexagonal unit cell.

Compound	Temperature (°C)	Phase	Lattice constants (Å or Å^2)
3b	RT[a]	Col_h	$a = 33.6$, $S = 978$
3c	RT[a]	Col_h	$a = 35.6$, $S = 1096$
	159	Col_h	$a = 33.0$, $S = 944$
3d	RT[a]	Col_h	$a = 37.5$, $S = 1219$
	160	Col_h	$a = 34.7$, $S = 1044$
3e	RT[b]	Col_h	$a = 39.1$, $S = 1325$
	160	Col_h	$a = 35.6$, $S = 1096$
3f	RT[a]	Col_h	$a = 41.7$, $S = 1505$
	150	Col_h	$a = 36.7$, $S = 1167$
3g	RT[a]	Col_h	$a = 45.4$, $S = 1784$
	136	Col_h	$a = 40.2$, $S = 1399$
3h	RT[a]	Col_h	$a = 47.9$, $S = 1988$
	139	Col_h	$a = 42.3$, $S = 1548$

[a] RT after cooling from the isotropic liquid.
[b] RT after heating up to a temperature slightly below the clearing point.

Two phenomena are observed at high temperatures: the hexagonal lattice constant a decreases compared to RT and (1 1) and (2 0) reflections are much weaker, to the point that they are masked by the background, so only the fundamental reflection could be measured. However, in spite of the disappearance of the higher order reflections, the mesophase is undoubtedly hexagonal columnar because no transitions are observed by optical microscopy or by differential scanning calorimetry (DSC) on cooling down to RT apart from the isotropic liquid to mesophase transition.

In the large-angle region of the patterns there is only a broad, diffuse halo characteristic of the melting of the hydrocarbon chains. This halo corresponds roughly to distances in the order of about 4.3–4.6 Å, with a tendency to larger values at high temperatures. In the case of **3h**, this halo is relatively sharp at RT and this suggests that the hydrocarbon chains of this compound are partially crystallised in spite of the above-mentioned absence of transition on cooling. It is noticeable that this compound, together with **3g**, yields a RT X-ray pattern with only one small-angle peak, suggesting some difficulties to adopt a well-organised mesomorphic hexagonal structure. However, the microscope textures and the above-mentioned evolution of the value of the constant a with the chain length support the assignation of the mesophase of **3g** and **3h** as hexagonal columnar.

It is interesting to discuss the organisation of these non-disc-like molecules in the columnar mesophase. These thiosemicarbazides have the possibility of intermolecular hydrogen bonds that allow for the generation of dimers or even aggregates containing several molecules (*31*). For building the columnar mesophase, groups of these dimers or aggregates are needed to constitute the supramolecular entity that stack into the columns. This phenomenon has been described for polycatenar liquid crystals (*32*), and in fact the compounds of the present series can be considered *biforked* mesogens (*32b*, *33*). Columnar mesophases generated by supramolecular aggregation through intermolecular hydrogen bonding have been reported (*13*, *18*).

The number Z of molecules that form the proposed supramolecular entity can be estimated by the equation,

$$Z = \frac{\rho V N_A}{M},$$

where ρ is the density, V is the unit cell volume, N_A is the Avogadro number and M is the molecular mass. The density in typical organic compounds has generally a value between 0.9 and 1 g cm^{-3}. In this case, with an important contribution of the hydrocarbon chains to the molecular mass, it is reasonable that the density is close to 0.9 g cm^{-3}. The unit cell volume is the area S of the 2D hexagonal lattice ($S = a^2 3^{1/2}/2$) multiplied by the mean stacking distance h. In these compounds h cannot be directly measured by X-ray measurements because the patterns do not contain any maximum corresponding to this parameter. This is not unexpected considering that the molecules of compounds **3b**–**h** are not in disc shape and the aggregates of molecules do not necessarily stack at a periodic repeating distance. However, we can consider that a group of Z molecules fills a column *slice* of thickness about 4–5 Å. Applying these consideration to the parameters obtained at RT, the above-mentioned equation predicts that seven molecules are needed to fill the cross-section of a column (Table S1 of the Supplementary Information, available online). Under this assumption, it is estimated that for **3b** seven molecules ($Z = 7$) occupies a height h of 5.2 Å and this value evolves in the series to 4.0 Å for **3h**. We could also predict that eight molecules ($Z = 8$) occupy a height of 6.0 Å for **3b** and evolve to 4.6 for **3h**. Another interpretation is to consider that an increasing number of molecules are needed to fill the same column height h upon lengthening the chain in the series. Both interpretations are complementary and in each case the decrease in h or the increase in Z is compensated by the increasing hexagonal lattice constant a.

The same conclusions can be qualitatively drawn from the high-temperature experiments. The shorter values for the hexagonal lattice constant a compared to RT are generally accepted as being related to the higher conformational disorder of the aliphatic chains. In turn the disordered chains require more space out of the mean plane perpendicular to the column axis and this must increase the height h of the column needed to accommodate the aggregates (Table S1 of the Supplementary Information, available online).

2.5 Ultraviolet–visible absorption and photoluminescence spectroscopy

The absorption and the emission of compounds **3a**–**h** in *N*,*N*-dimethylformamide (DMF) are depicted in Figure S2 (Supporting Information, available online), and the photophysical data are summarised in Table 3. Similar absorption patterns were observed for all these compounds, and all of them exhibit an intense absorption band at 331–332 nm. In solution in DMF all the compounds displayed one emission band at 361–365 nm on excitation at RT at the absorption maximum. Photoluminescence is observed for all the compounds in DMF solutions with quantum yields (ϕ_{PL}) ranging from 3.5% to 5%. The emission colours of these compounds are all in the purple region.

The photoluminescence quantum yield, ϕ_{PL}, was calculated according to the equation:

$$\phi_{PL} \approx \phi_{std} \times \left(\frac{Abs_{std}}{Abs_{sample}} \times \frac{A_{sample}}{A_{std}} \times \frac{\eta^2_{sample}}{\eta^2_{std}} \right),$$

Table 3. Absorption and photoluminescence spectra of compounds **3a**–**h**.

Compound	$\lambda_{abs\,max}$[a]/nm ($\varepsilon = 3.928 \times 10^3$)[b]	$\lambda_{em\,max}$[c]/nm	% ϕ_{PL}[d]	Stokes shift/nm
3a ($n = 5$)	332.0	365.1	4.7	33.1
3b ($n = 6$)	332.0	362.0	4.1	30.0
3c ($n = 7$)	331.0	361.1	3.5	30.1
3d ($n = 8$)	330.0	362.0	3.6	32.0
3e ($n = 9$)	331.0	364.0	4.2	33.0
3f ($n = 10$)	331.0	362.0	5.0	31.0
3g ($n = 12$)	331.0	361.1	4.2	30.1
3h ($n = 14$)	331.0	363.1	4.2	32.1

[a] Measured in DMF.
[b] Units = $M^{-1}\,cm^{-1}$.
[c] Excited at absorption maxima.
[d] Standard 9,10-diphenylantracene.

where ϕ_{PL} is the photoluminescence quantum yield of the standard 9,10-diphenylantracene ($\phi_{std} = 0.950$, ethanol); Abs_{std} and Abs_{sample} are the absorbance of the standard and sample, respectively; A_{sample} and A_{std} are the integrated area of the emission peak of the sample and standard, respectively; η_{sample} and η_{std} are the refractive indices of the sample and standard solutions (pure solvents were assumed), respectively. The quantum yields and the Stokes shifts are summarised in Table 3.

2.6 FT-IR measurements

In order to examine the presence of the intermolecular hydrogen bonding, the temperature-dependent FT-IR spectra of compound **3f** have been recorded on heating at three different temperatures: at 17°C (crystal phase), at 140°C (Cr-mesophase transition) and at 170°C (Col_h mesophase), as is shown in Figure 3.

At RT (17°C), **3f** exhibits the characteristic bands of N—H stretching vibrations of the terminal amino group at 3150–3233 cm^{-1} and the central NH group at 3409 cm^{-1}, and the carbonyl group at 1657 cm^{-1}. On heating, these bands increase in intensity and shift to higher wavenumbers. Thus the carbonyl band appears at 1660 cm^{-1} at 140°C, 1663 cm^{-1} at 170°C (Figure 3(a)). The central NH band appears at 3410 cm^{-1} at 140°C, and at 3412 cm^{-1} at 170°C. In addition, the N—H stretching bands of the terminal amino group also show a shift by about 3 cm^{-1} (Figure 3(b)). These observations suggest the formation of the intermolecular hydrogen bonding between C═O, C═S, NH and NH_2 groups. It is suggested that the amide N—H groups are associated with C═S group *via* N—H···S═C intermolecular hydrogen bond-generating dimers, which are associated with other dimers through intermolecular interactions of the NH_2 groups with C═O groups *via* N—H···O═C hydrogen bonding (*31*). These intermolecular hydrogen bonds promote molecular ordering and stability of the liquid crystalline phase, explaining the appearance of columnar mesophases.

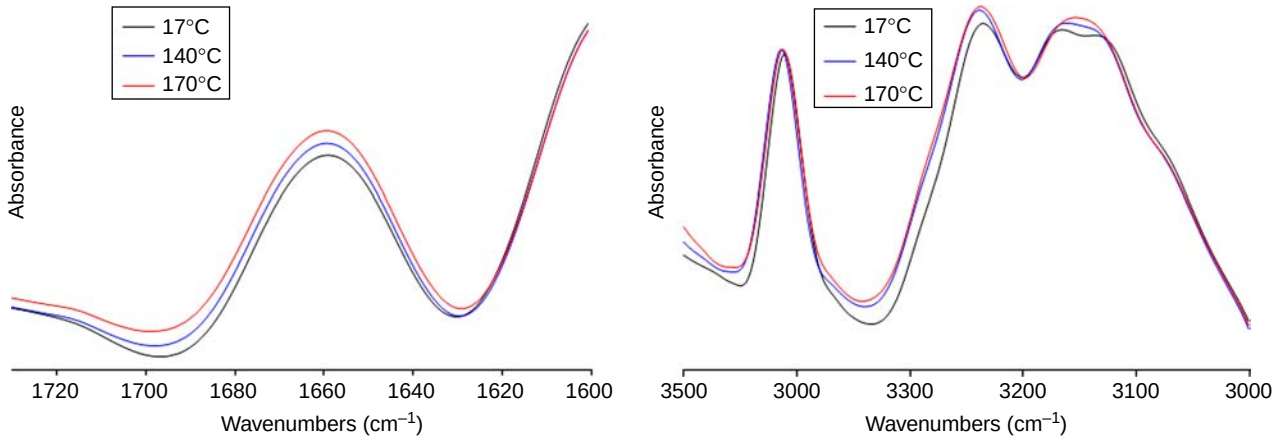

Figure 3. FT-IR spectra (NaCl crystal plates) for compound **3f**: 1720–1600 cm^{-1} regions (a) and 3500–3000 cm^{-1} regions (b) at 17, 140 and 170°C.

3. Experimental section

3.1 General

^{1}H and ^{13}C NMR spectra were recorded using a Bruker Avance 400 MHz spectrometer with DMSO-d_6 as solvent and tetramethylsilane (TMS) as an internal standard. FT-IR spectra were recorded with a Nicolet Magna 550 spectrometer. Samples were pressed tablets with KBr. The samples for hydrogen bond study at various temperatures were sandwiched between two NaCl crystal plates. The sandwiched samples were held on a hot stage equipped with a temperature controller. Electrospray-ionisation ion trap mass spectra (ESI-MS) were recorded on Bruker ion trap 3000 spectrometer.

Transition temperatures and textures of mesophases were determined by POM using an Olympus BX51 optical microscope equipped with an Olympus UAN360P polariser and an Instec HCS302 heat stage.

Transition temperatures and enthalpies were investigated by DSC using a Rheometric DSC-V calorimeter. Samples were encapsulated in aluminium pans and observed at scanning rate of 5°C min^{-1} on heating and cooling. The instrument was calibrated using an indium standard (156.6°C, 28.44 J g^{-1}) under nitrogen atmosphere. The purity of the final products was evaluated by thin layer chromatography.

The mesophases were investigated by XRD. The XRD patterns were obtained with a pinhole camera (Anton-Paar, Graz, Austria) operating with a point-focused Ni-filtered Cu Kα beam. The samples were held in the Lindemann glass capillaries (0.9 mm diameter). The patterns were collected on flat photographic film perpendicular to the X-ray beam. Spacing was obtained *via* Bragg's law.

TGAs of solid samples of **3a**–**h** were performed by TA Instruments (New Castle, Delaware, USA) Q5000IR under a stream of flowing N_2.

Ultraviolet–visible absorbance measurements were made with Varian Cary 50 instrument between 350 and 900 nm. Luminescence measurements were obtained using a Varian Cary Eclipse Fluorescence spectrophotometer. Spectra of the pure compounds were recorded in 1×10^{-4} mol/l DMF solutions under excitation at the absorption maximum.

3.2 Synthesis and characterisation

3.2.1 Synthesis of the methyl 3,4-n-dialkoxybenzoates (1a–h)

All derivatives were prepared similarly according to the procedure described in Ref. (*29*).

General method. Anhydrous K_2CO_3 (59 mmol) and methyl 3,4-dihydroxybenzoate (19.5 mmol) were added to a deoxygenated mixture of DMF (80 ml) and of 1-bromodecane (39 mmol) under nitrogen atmosphere. After TLC analysis, the mixture was heated at 80°C for 10 h. The reaction mixture was cooled to RT, water (100 ml) was added, and the product was extracted with diethyl ether. The combined organic extracts were washed with water and dried over $MgSO_4$. After filtration, the solvent was evaporated under reduced pressure, and the crude product was passed through a column of silica gel using 2% ethyl acetate in hexane as eluent to afford **1a**–**f** as white solids.

Compound	**1a**	**1b**	**1c**	**1d**	**1e**	**1f**	**1g**	**1h**
Melting point (°C)	Liquid	Liquid	Liquid	47	55	45	52	64
Yield (%)	85	79	81	83	81	86	80	85

The spectroscopic characterisation of **1f** as a representative example is given:

^{1}H NMR ($CDCl_3$, TMS, 400 MHz): $\delta = 0.91$ (t, 6H, $2CH_3$) 1.29–1.53 (m, 36H, $18CH_2$); 1.82–1.90 (m, 4H, $2CH_2$); 3.91 (s, 3H, CH_3); 4.07 (m, 4H, 2 —OCH_2); 6.98 (d, $J = 8.4$ Hz, 1H, H aromatic); 7.56 (d, $J = 1.9$ Hz, 1H, H aromatic); 7.66 (dd, $J = 8.4$ Hz, 1H, H aromatic).

^{13}C NMR ($CDCl_3$, TMS, 100.6 MHz): $\delta = 14.1$, 22.7, 26.0, 26.1, 29.1, 29.2, 29.4, 29.5, 29.7, 31.9, 51.8, 64.9 (aliphatic C); 51.9 (OCH_3); 69.0 and 69.3 (2 —OCH_2); 111.9, 114.3, 123.5 (aromatic CH); 122.4, 148.5, 153.2 (quaternary aromatic C); 167.0 (C═O).

FT-IR (KBr, cm^{-1}): 2921, 2850 (C sp^3-H); 1714 (C═O); 1215 (C—O).

3.2.2 Synthesis of the 3,4-n-dialkoxyphenylhydrazides (2a–h)

All derivatives were prepared similarly according to the procedure described elsewhere (*24*, *25*, *29*).

General method. A solution of the corresponding compound of series **1a**–**h** (11 mmol) and an excess of hydrazine monohydrate in ethanol (100 ml) was heated to 80°C for 32 h. Then water (80 ml) was added and the resulting precipitate was collected, dried under vacuum and recrystallised from ethanol to yield pure **2a**–**h** compounds as white solids.

Compound	**2a**	**2b**	**2c**	**2d**	**2e**	**2f**	**2g**	**2h**
Melting point (°C)	103	99	102	104	107	105	101	100
Yield (%)	82	78	76	79	74	86	80	83

The spectroscopic characterisation of **2f** as a representative example is given:

^{1}H NMR (DMSO-d_6, TMS, 400 MHz): $\delta = 0.87$ (t, 3H, CH_3); 0.89 (t, 3H, CH_3); 1.29–1.44 (m, 8H, $4CH_2$); 1.66–1.74 (m, 4H, $2CH_2$); 3.96 (m, 4H, 2 $-OCH_2$); 4.41 (s, 2H, NH_2); 6.97 (d, $J = 8.9$ Hz, 1H, H aromatic); 7.40–7.42 (m, 2H, H aromatic); 9.59 (s, 1H, NH).

^{13}C NMR (DMSO-d_6, TMS, 100.6 MHz): $\delta = 14.3$, 22.3, 26.0, 26.1, 28.2, 29.1, 29.2, 29.4, 29.5, 29.7, 31.9, 51.8, 64.9 (aliphatic C); 68.7 and 68.9 (2 $-OCH_2$); 112.7, 113.0, 120.8 (aromatic CH); 126.0, 148.4, 151.4 (quaternary aromatic C); 166.0 (C=O).

FT-IR (KBr, cm^{-1}): 3311, 3254 ($-$NH and $-NH_2$); 2920, 2852 (C sp^3-H); 1617 (C=O).

3.2.3 *Synthesis of 3,4-*n-*dialkoxybenzoylthiosemicarbazides (**3a**–**h**)*

All derivatives were prepared similarly according to the procedure described previously by us (*24*, *25*).

General method. The corresponding 3,4-*n*-dialkoxyphenylhydrazide (series **2a**–**h**; 6.7 mmol) was suspended in 20 ml of alcoholic hydrogen chloride solution and evaporated under reduced pressure; the residue was heated under reflux for 30 h with a solution of dry ammonium thiocyanate (7.4 mmol) in absolute ethanol. The solid was filtered off, washed several times with water and recrystallised from ethanol to yield pure **3a**–**h** compounds as white solids.

Compound	**3a**	**3b**	**3c**	**3d**	**3e**	**3f**	**3g**	**3h**
Yield (%)	80	75	76	88	93	85	90	93

Compound **3a**. ^{1}H NMR (DMSO-d_6, TMS, 400 MHz): $\delta = 0.84$ (t, 6H, $2CH_3$); 1.24–1.69 (m, 12H, $6CH_2$); 3.99 (t, 4H, 2 $-OCH_2$); 6.98 (d, $J = 8.2$ Hz, 1H, H aromatic); 7.46 (d, $J = 7.3$ Hz, 2H, H aromatic); 7.56 and 7.86 (s, 2H, S=C$-NH_2$); 9.29 (s, 1H, S=C$-$NH); 10.2 (s, 1H, O=C$-$NH).

^{13}C NMR (DMSO-d_6, TMS, 100.6 MHz): $\delta = 14.3$, 22.5, 26.0, 26.1, 29.1, 29.2, 29.4, 29.5, 31.8 (aliphatic C); 68.7 and 69.0 (2 $-OCH_2$); 112.7, 113.5, 121.9 (aromatic CH); 125.1, 148.2, 152.0 (quaternary aromatic C); 165.8 (C=O); 182.6 (C=S).

FT-IR (KBr, cm^{-1}): 3416 ($-$NH); 3251, 3178 ($-NH_2$); 2947 and 2863 (C sp^3-H); 1668 (C=O); 1268 (C=S); 1217 (C$-$O).

ESI: $C_{18}H_{29}N_3O_3S$ calculated: 367.19; found: 367.10.

Compound **3b**. ^{1}H NMR (DMSO-d_6, TMS, 400 MHz): $\delta = 0.84$ (t, 6H, $2CH_3$); 1.24–1.69 (m, 16H, $8CH_2$); 3.99 (t, 4H, 2 $-OCH_2$); 6.98 (d, $J = 8.2$ Hz, 2H, H aromatic); 7.46 (d, $J = 7.3$ Hz, 2H, H aromatic); 7.56 and 7.86 (s, 2H, S=C$-NH_2$); 9.29 (s, 1H, S=C$-$NH); 10.2 (s, 1H, O=C$-$NH).

^{13}C NMR (DMSO-d_6, TMS, 100.6 MHz): $\delta = 14.3$, 22.5, 26.0, 26.1, 29.1, 29.2, 29.4, 29.5, 31.8 (aliphatic C); 68.7 and 69.0 (2 $-OCH_2$); 112.7, 113.5, 121.9 (aromatic CH); 125.1, 148.2, 152.0 (quaternary aromatic C); 165.8 (C=O); 182.6 (C=S).

FT-IR (KBr, cm^{-1}): 3417 ($-$NH); 3250, 3174 ($-NH_2$); 2927, 2860 (C sp^3-H); 1668 (C=O); 1266 (C=S); 1217 (C$-$O).

ESI: $C_{20}H_{33}N_3O_3S$ calculated: 395.22; found: 394.90.

Compound **3c**. ^{1}H NMR (DMSO-d_6, TMS, 400 MHz): $\delta = 0.86$ (t, 6H, $2CH_3$); 1.27–1.70 (m, 20H, $10CH_2$); 3.98 (t, 4H, 2 $-OCH_2$); 6.99 (d, $J = 8.8$ Hz, 1H, H aromatic); 7.47 (d, $J = 7.1$ Hz, 2H, H aromatic); 7.55 and 7.85 (s, 2H, S=C$-NH_2$); 9.28 (s, 1H, S=C$-$NH); 10.2 (s, 1H, O=C$-$NH).

^{13}C NMR (DMSO-d_6, TMS, 100.6 MHz): $\delta = 14.3$, 22.5, 25.9, 26.0, 28.9, 29.1, 29.2, 31.7 (aliphatic C); 68.7 and 69.0 (2 $-OCH_2$); 112.8, 113.6, 121.9 (aromatic CH); 125.1, 148.2, 152.0 (quaternary aromatic C); 165.8 (C=O); 182.5 (C=S).

FT-IR (KBr, cm^{-1}): 3417 ($-$NH); 3250, 3174 ($-NH_2$); 2927, 2860 (C sp^3-H); 1668 (C=O); 1266 (C=S); 1217 (C$-$O).

ESI: $C_{22}H_{37}N_3O_3S$ calculated: 423.20; found: 423.14.

Compound **3d**. ^{1}H NMR (DMSO-d_6, TMS, 400 MHz): $\delta = 0.84$ (t, 6H, $2CH_3$); 1.24–1.69 (m, 24H, $12CH_2$); 3.99 (t, 4H, 2 $-OCH_2$); 6.98 (d, $J = 8.2$ Hz, 1H, H aromatic); 7.46 (d, $J = 7.3$ Hz, 2H, H aromatic); 7.56 and 7.86 (s, 2H, S=C$-NH_2$); 9.29 (s, 1H, S=C$-$NH); 10.2 (s, 1H, O=C$-$NH).

^{13}C NMR (DMSO-d_6, TMS, 100.6 MHz): $\delta = 14.3$, 22.5, 26.0, 26.1, 29.1, 29.2, 29.4, 29.5, 31.8 (aliphatic C); 68.7 and 69.0 (2 $-OCH_2$); 112.7, 113.5, 121.9 (aromatic CH); 125.1, 148.2, 152.0 (quaternary aromatic C); 165.8 (C=O); 182.6 (C=S).

FT-IR (KBr, cm^{-1}):3416 ($-$NH); 3252, 3178 ($-NH_2$); 2920, 2851 (C sp^3-H); 1666 (C=O); 1268 (C=S); 1219 (C$-$O).

ESI: $C_{24}H_{41}N_3O_3S$ calculated: 451.28; found: 451.28.

Compound **3e**. ^{1}H NMR (DMSO-d_6, TMS, 400 MHz): $\delta = 0.85$ (t, 6H, $2CH_3$); 1.25–1.70 (m, 28H, $14CH_2$); 3.99 (t, 4H, 2 $-OCH_2$); 6.99 (d, $J = 8.9$ Hz, 1H, H aromatic); 7.46 (d, $J = 7.4$ Hz, 2H, H aromatic); 7.55 and 7.84 (s, 2H, S=C$-NH_2$); 9.27 (s, 1H, S=C$-$NH); 10.1 (s, 1H, O=C$-$NH).

^{13}C NMR (DMSO-d_6, TMS, 100.6 MHz): $\delta = 14.3$, 22.5, 25.5, 26.0, 26.1, 29.1, 29.2, 29.4, 29.5, 31.7 (aliphatic C); 68.7 and 69.0 (2 $-OCH_2$); 112.6, 113.5, 121.8 (aromatic CH); 125.1, 148.2, 152.0 (quaternary aromatic C); 165.8 (C=O); 182.5 (C=S).

FT-IR (KBr, cm^{-1}): 3416 ($-$NH); 3252, 3178 ($-NH_2$); 2920, 2851 (C sp^3-H); 1666 (C=O); 1268 (C=S); 1219 (C$-$O).

ESI: $C_{26}H_{45}N_3O_3S$ calculated: 479.31; found: 479.23.

Compound **3f**. ^{1}H NMR (DMSO-d_6, TMS, 400 MHz): $\delta = 0.84$ (t, 6H, $2CH_3$); 1.24–1.69 (m, 32H, $16CH_2$); 3.99 (t, 4H, 2 $-OCH_2$); 6.98 (d, $J = 8.2$ Hz, 1H, H aromatic); 7.46 (d, $J = 7.3$ Hz, 2H, H aromatic); 7.56 and 7.86 (s, 2H, S=C$-NH_2$); 9.29 (s, 1H, S=C−NH); 10.2 (s, 1H, O=C−NH).

^{13}C NMR (DMSO-d_6, TMS, 100.6 MHz): $\delta = 14.3$, 22.5, 26.0, 26.1, 29.1, 29.2, 29.4, 29.5, 31.8 (aliphatic C); 68.7 and 69.0 (2 $-OCH_2$); 112.7, 113.5, 121.9 (aromatic CH); 125.1, 148.2, 152.0 (quaternary aromatic C); 165.8 (C=O); 182.6 (C=S).

FT-IR (KBr, cm^{-1}): 3417 (−NH); 3250, 3178 ($-NH_2$); 2920, 2852 (C sp^3-H); 1667 (C=O); 1267 (C=S); 1218 (C−O).

ESI: $C_{28}H_{49}N_3O_3S$ calculated: 507.35; found: 507.34.

Compound **3g**. ^{1}H NMR (DMSO-d_6, TMS, 400 MHz): $\delta = 0.84$ (t, 6H, $2CH_3$); 1.24–1.69 (m, 40H, $20CH_2$); 3.99 (t, 4H, 2 $-OCH_2$); 6.98 (d, $J = 8.2$ Hz, 1H, H aromatic); 7.46 (d, $J = 7.3$ Hz, 2H, H aromatic); 7.56 and 7.86 (s, 2H, S=C$-NH_2$); 9.29 (s, 1H, S=C−NH); 10.2 (s, 1H, O=C−NH).

^{13}C NMR (DMSO-d_6, TMS, 100.6 MHz): $\delta = 14.3$, 22.5, 26.0, 26.1, 29.1, 29.2, 29.4, 29.5, 31.8 (aliphatic C); 68.7 and 69.0 (2 $-OCH_2$); 112.7, 113.5, 121.9 (aromatic CH); 125.1, 148.2, 152.0 (quaternary aromatic C); 165.8 (C=O); 182.6 (C=S).

FT-IR (KBr, cm^{-1}):3416 (−NH); 3252, 3178 ($-NH_2$); 2920, 2851 (C sp^3-H); 1666 (C=O); 1268 (C=S); 1219 (C−O).

ESI: $C_{32}H_{57}N_3O_3S$ calculated: 563.41; found: 563.37.

Compound **3h**. ^{1}H NMR (DMSO-d_6, TMS, 400 MHz): $\delta = 0.84$ (t, 6H, $2CH_3$); 1.24–1.69 (m, 48H, $24CH_2$); 3.99 (t, 4H, 2 $-OCH_2$); 6.98 (d, $J = 8.2$ Hz, 1H, H aromatic); 7.46 (d, $J = 7.3$ Hz, 2H, H aromatic); 7.56 and 7.86 (s, 2H, S=C$-NH_2$); 9.29 (s, 1H, S=C−NH); 10.2 (s, 1H, O=C−NH).

^{13}C NMR (DMSO-d_6, TMS, 100.6 MHz): $\delta = 14.3$, 22.5, 26.0, 26.1, 29.1, 29.2, 29.4, 29.5, 31.8 (aliphatic C); 68.7 and 69.0 (2 $-OCH_2$); 112.7, 113.5, 121.9 (aromatic CH); 125.1, 148.2, 152.0 (quaternary aromatic C); 165.8 (C=O); 182.6 (C=S).

FT-IR (KBr, cm^{-1}): 3416 (−NH); 3252, 3178 ($-NH_2$); 2920, 2851 (C sp^3-H); 1666 (C=O); 1268 (C=S); 1219 (C−O).

ESI: $C_{36}H_{65}N_3O_3S$ calculated: 619.47; found: 619.5.

Acknowledgements

This work was supported by FONDECYT (1100140), CONICYT, FULLBRIGHT, 'Dirección de Investigación' of the University of Concepción. We thank Dr David King for his help in measuring the mass spectra in the laboratory in the Department of Molecular and Cell Biology and Department of Chemical and Biomolecular Engineering, 'Howard Hughes Medical Institute', University of California and Miguel Modestino for his collaboration in the measurements of physical parameters in the Department of Chemical and Biomolecular Engineering of the University of California, Berkeley. J.B. thanks the Spanish project CTQ2009-09030.

References

(1) Lehn, J.M. *Angew. Chem. Int. Ed. Engl.* **1988**, *27*, 89–112.
(2) Shen, H.; Jeong, K.-U.; Xiong, H.; Graham, M.J.; Leng, S.; Zheng, J.X.; Huang, H.; Guo, M.; Harris, F.W.; Cheng, S.Z.D. *Soft Matter* **2006**, *2*, 232–242.
(3) Kato, T.; Fréchet, J.M. *J. Am. Chem. Soc.* **1989**, *111*, 8533–8534.
(4) Kato, T.; Adachi, H.; Fujishima, A.; Fréchet, J.M.J. *Chem. Lett.* **1992**, 265–268.
(5) Paleos, C.M. *Mol. Cryst. Liq. Cryst.* **1994**, *243*, 159–183.
(6) Paleos, C.M.; Tsiourvas, D. *Liq. Cryst.* **2001**, *28*, 1127–1161.
(7) Kato, T.; Mizoshita, N.; Kishimoto, K. *Angew. Chem. Int. Ed.* **2006**, *45*, 38–68.
(8) Joachimi, D.; Tschierske, C.; Müller, H.; Wendorff, J.H.; Schneider, L.; Kleppinger, R. *Angew. Chem. Int. Ed. Engl.* **1993**, *32*, 1165–1167.
(9) Kölbel, M.; Beyersdorff, T.; Cheng, X.H.; Tschierske, C.; Kain, J.; Diele, S. *J. Am. Chem. Soc.* **2001**, *123*, 6809–6818.
(10) Kohmoto, S.; Someya, Y.; Kishikawa, K. *Liq. Cryst.* **2010**, *37*, 209–216.
(11) Paraschiv, I.; Tomkinson, A.; Giesbers, M.; Sudhölter, E.J.; Zuilhof, H.; Marcelis, A.T. *Liq. Cryst.* **2007**, *34*, 1029–1038.
(12) Brunsveld, L.; Folmer, B.J.B.; Meijer, E.W.; Sijbesma, R.P. *Chem. Rev.* **2001**, *101*, 4071–4097.
(13) Jeong, M.J.; Park, J.H.; Lee, C.; Chang, J.Y. *Org. Lett.* **2006**, *8*, 2221–2224.
(14) Demus, D.; Gloza, A.; Hauser, H.; Rapthel, I.; Wiegeleben, A. *Cryst. Res. Technol.* **1981**, *16*, 1445–1451.
(15) Wang, H.; Bai, B.; Pang, D.; Zou, Z.; Xuan, L.; Li, F.; Zhang, P.; Liu, L.; Long, B.; Li, M. *Liq. Cryst.* **2008**, *35*, 333–338.
(16) Zhang, P.; Qu, S.; Bai, B.; Wang, H.; Ran, X.; Zhao, C.; Li, M. *Liq. Cryst.* **2009**, *36*, 817–824.
(17) Kutsumizu, S. *Curr. Opin. Solid State Mater. Sci.* **2002**, *6*, 537–543.
(18) Beginn, U. *Prog. Polym. Sci.* **2003**, *28*, 1049–1105.
(19) Parra, M.; Hidalgo, P.; Barberá, J.; Carrasco, E.; Saavedra, C. *Liq. Cryst.* **2006**, *33*, 391–397.
(20) Liu, J.; Yi, W.; Wan, Y.; Ma, L.; Song, H. *Bioorg. Med. Chem.* **2008**, *16*, 1096–1102.
(21) Wang, X.C.; Wang, J.K.; Li, Z. *Chin. Chem. Lett.* **2004**, *15*, 635–638.
(22) Wei, T.B.; Zhang, Y.M.; Wang, H.; Gao, L.M. *Phosphorus Sulfur Silicon* **2004**, *179*, 1539–1544.
(23) Li, J.P.; Luo, Q.F.; Wang, Y.L.; Wang, H. *Synth. Commun.* **2001**, *31*, 1793–1797.
(24) Parra, M.; Belmar, J.; Zunza, H.; Zúñiga, C.; Villouta, S.H.; Martínez, R. *J. Prakt. Chem.* **1995**, *337*, 325–327.
(25) Parra, M.; Hernández, S.; Alderete, J.; Zúñiga, C. *Liq. Cryst.* **2000**, *27*, 995–1000.
(26) Xue, C.; Jin, S.; Weng, X.; Ge, J.J.; Shen, Z.; Shen, H.; Graham, M.J.; Jeong, K.U.; Wang, H.; Zhang, D.; Guo, M.; Harris, F.W.; Cheng, S.Z.D.; Li, C.Y.; Zhu, L. *Chem. Mater.* **2004**, *16*, 1014–1025.
(27) Keinan, S.; Ratner, M.A.; Mark, T.J. *Chem. Mater.* **2004**, *16*, 1848–1854.
(28) Zhang, Y.; Jiang, J.; Sun, X.; Xue, Q. *Aust. J. Chem.* **2009**, *62*, 455–463.

(29) Zhang, Y-D.; Jespersen, K.G.; Kempe, M.; Kornfield, J.A.; Barlow, S.; Kippelen, B.; Marder, S.R. *Langmuir* **2003**, *19*, 6534–6536.
(30) Barberá, J.; Godoy, M.A.; Hidalgo, P.I.; Parra, M.L.; Ulloa, J.A.; Vergara, J.M. *Liq. Cryst.* **2011**, *38*, 679–688.
(31) Boechat, N.; Lages, A.; Kover, W.B.; Wardell, S.M.V.; Skakle, J.M.S. Acta Cryst. *E* **2006**, *62*, 2563–2565.
(32) (a) Malthête, J.; Levelut, A.M.; Nguyen, H.T. *J. Phys. Lett*. **1985**, *46*, 875–880; (b) Gharbia, M.; Charbi, A.; Nhuyen, H. T.; Malthête, J. *Curr. Opin. Colloid Interface Sci*. **2002**, *7*, 312–315; (c) Huck, D.M.; Nguyen, H.L.; Horton, P.N.; Hursthouse, M.B.; Guillon, D.; Bonnio, B.; Bruce, D.W. *Polyhedron* **2006**, *25*, 307–324; (d) Qu, S.; Li, M. *Tetrahedron* **2007**, 63, 12429–12436; (e) Choi, J.W.; Han, J.H.; Ryu, M.H.; Cho, B.K. *Bull. Korean Chem. Soc*. **2011**, *32*, 781–782.
(33) Nguyen, H.T.; Destrade, C.; Levelut, A.M.; Malthête, J. *J. Phys. Paris* **1986**, *47*, 553–557.